Adaptive Control of Voltage Source Converter Based Scheme for Power Quality Improved Grid-Interactive Solar PV- Battery System

Ujjwal Kumar Kalla, *Senior Member, IEEE*, Hemant Kaushik, *Student Member, IEEE*,
Bhim Singh, *Fellow IEEE* and Shailendra Kumar, *Member, IEEE*
Department of Electrical Engineering, Govt. Engineering College Bikaner, Rajasthan, India
Department of Electrical Engineering, Indian Institute of Technology Delhi, India
ukkalla@gmail.com, hemantkkaushik@gmail.com, bhimsinghiitd61@gmail.com, er.dwivedi88@gmail.com

***Abstract*— This paper presents an implementation of an Adaptive Learning Based Back Propagation (AL-BP) control technique for improved power quality grid interactive solar PV - battery supported system catering the balanced and unbalanced three phase four wire (3P-4W) nonlinear loads and single phase loads of various nature simultaneously. Moreover the source currents remain balanced and sinusoidal for all operating and loading conditions such as in highly unbalance loading conditions where a load on one of the phase is disconnected. An AL-BP control technique is used to control the voltage at point of common coupling and to improve power quality under various loading conditions through mitigation of harmonic currents, reactive power compensation, active power balancing and neutral current compensation in the 3P-4W system. It also improves the system power factor in highly nonlinear and unbalanced loading conditions. The AL-BP control scheme has the capability to self tune the arbitrary nonlinear systems such as grid-interactive critically unbalanced 3-phase 4-wire system feeding highly nonlinear loading systems. Therefore, the proposed control technique is found capable of dealing with above said large unknown-nonlinearity of 3-phase 4-wire system. This scheme significantly improves the steady state and dynamic performances of the 3 phase 4 wire (3P-4W) grid interactive solar PV - battery supported system. The proposed AL-BP control technique has been implemented using DSP processor in real time in order to validate the claims.**

Index Terms— ***Solar PV, VSC, power quality, non-linear loads, integrated system.***

NOMENCLATURE

Quantity	
i_{sR}	Source current in phase R
i_{sY}	Source current in phase Y
i_{sB}	Source current in phase B
i_{sn}	Source neutral current
i_{lR}	Load current in phase R
i_{lY}	Load current in phase Y
i_{lB}	Load current in phase B
i_{ln}	Load neutral current
i_{vscR}	VSC current in Phase R
i_{vscY}	VSC current in Phase Y
i_{vscB}	VSC current in Phase B
i_{vscn}	VSC neutral current
V_{DC}	DC link voltage
V_{pv}	Solar PV voltage
I_{pv}	Solar PV current
THD	Total Harmonic Distortion

Manuscript received March 15, 2019; revised June 14, 2019; accepted September 09, 2019.

Ujjwal Kumar Kalla and Hemant Kaushik are with the Department of Electrical Engineering, Govt. Engineering College Bikaner, Rajasthan, India - 334004, Bhim Singh and Shailendra Kumar are with the Department of Electrical Engineering, Indian Institute of Technology Delhi, New Delhi-110016,INDIA (e-mail: ukkalla@gmail.com, hemantkkaushik@gmail.com, bhimsinghiitd61@gmail.com, er.dwivedi88@gmail.com).

.

I. INTRODUCTION

DUE to serious environmental concerns, advancement in the technologies and decrease in price, the Solar-Photovoltaic (PV) based power generation has increased during last few years. A large amount of green house gases is generated by the thermal power plants. The easy availability of solar energy irrespective of the geographical location, the electric power-generation using solar-photovoltaic plants, has been found better and more suitable in comparison to other electrical power generation systems based on renewable energy sources. Conventional self tuning adaptive control systems are more suitable for linear systems or some specific non linear systems [1]. The neural network algorithm is often used in recent years for nonlinear adaptive filtering based systems [2]. An adaptive load shading scheme using an adaptive artificial neural network, and its transient stability analysis for electrical utility systems have been presented in [3]. A back propagation neural network based training scheme has been discussed in [4]. A back propagation through time base learning algorithm and a new recurrent adaptive control theory have been presented in [5]. A back propagation neutral network is proposed in [6] for nonlinearity compensation in optical current sensors based photonic transducer systems. An adaptive output tracking architecture is proposed in [7] for a

three layered neutral network system, which is used to train to the nonlinear plants. An adaptive wavelet neural network to determine dynamic transfer capability of electricity market, has been presented in [8]. The possibility of using a simple approximation for estimating the error using the back propagation neural network is presented in [9]. A nonlinear adaptive neural network based control for multivariable motion control systems has been discussed in [10]. An adaptive back propagation based learning scheme for analog neural networks has been presented in [11]. The modeling of switched reluctance motor using an adaptive neuro fuzzy system has been presented in [12]. The hybrid learning scheme used in this paper, combines the linear least squares estimation methods and a back propagation algorithm. Various types of adaptive neutral networks for control systems have been discussed in [13]. The development of an auto reclosing system using adaptive control based on optimized neutral network has been proposed in [14]. A direct adaptive neutral based control scheme for synchronous generators has been presented in [15]. A back propagation neural network based control algorithm for resonator bank structure has been presented in [16]. An optimum adaptive learning scheme for error back propagation networks has been proposed in [17]. A new control algorithm for three phase four wire shunt and series active filter for unbalanced system is reported in [18]. Ryan et al. [19] have proposed a three phase four wire inverter and controller for unbalanced system using a new decoupling quad transformation matrix. A new power quality improved multifunctional three phase four wire grid connected compensator is reported in [20]. Zeng et al. [21] have proposed a modular multifunctional distributed generation unit using 3H bridge converter to enhance the power quality in low voltage systems. A novel adaptive fuzzy logic and hysteresis controller using three phase four wire full bridge inter-leaved buck active power filter for high power applications is presented in [22]. Karimi et al. [23-24] proposed a new decentralized control method for power management and load sharing in islanded micro-grid. Merabet et al. [25] have developed an energy management and control algorithm for standalone micro-grid which consists of hybrid resources such as PV solar, wind and battery energy storage system. An optimal power flow technique of a photo-voltaic battery powered fast electric vehicles charging stations is presented in [26].

This paper presents an AL-BP control technique for improved power quality grid interactive solar PV - battery supported system. The proposed power quality improved system is capable of delivering highly non-sinusoidal currents to nonlinear and unbalance loads of different types such that single and three phase industrial and domestic loads, while the source currents in all three phases remains balanced and sinusoidal for all operating and loading conditions. The proposed AL-BP control technique has been implemented using DSP processor in real time in order to validate the claims.

II. Scheme and Working Principle

The block diagram of proposed power quality improved AL-BP control based 3 phase 4 wire grid-interactive solar-PV battery system is presented in Fig. 1(a). The photograph of the experimental proto type is shown in Fig 1(b). The proposed system operates in three phase balanced mode of operation while feeding highly unbalanced and nonlinear loads. The proposed scheme consists of a four leg IGBT based voltage source converter (VSC), three inductors for interfacing between grid and VSC, a solar-PV array, a boost converter for MPPT, a 3-phase RC filter, a battery energy storage, a DC bus capacitor and a bidirectional DC-DC converter for battery charging. The AC side of VSC is connected to the grid through interfacing inductor and fourth leg of VSC is connected to the neutrals of both source (grid) and load. The fourth leg of VSC supplies all the harmonic currents demanded by the neutral of the load. Therefore, load does not demand any harmonic current from neutral of the grid, which in turn significantly reduces the losses in neutral wire of source/grid and also improves the power quality of the three phase four wire system in critically unbalanced loading conditions. The proposed control algorithm is implemented using a DSP based controller that generates the desired gating pulses for all eight IGBT switches of four leg voltage source converter in order to achieve the desired performance. The VSC is controlled through adaptive learning based back propagation control technique [27-29] based control scheme. The incremental conductance algorithm is used for maximum power point tracking [30-31]. The bidirectional converter is used to control the flow of battery power during charging or discharging. The VSC supplies adjustable reactive power to the grid in order to maintain a constant system voltage at point of common coupling (PCC). The 4 leg VSC operates the system at almost unity power factor and compensates reactive and harmonic currents demanded by the load, therefore, it improves the system power quality significantly.

III. Control Algorithm

The AL-BP Algorithm for battery supported improved power quality three phase four wire (3P4W) system, is used for extraction of fundamental real and imaginary power components of load currents of all phases [31].

A. Adaptive Learning Back Propagation Based Control Algorithm

The mathematical-modeling of proposed AL-BP control algorithm is as follows.

The voltage (V_T) at point of common coupling is estimated as,

$$V_T = \sqrt{\frac{2}{3} \times \left({V_{phR}}^2 + {V_{phY}}^2 + {V_{phB}}^2 \right)} \tag{1}$$

In-phase normalized signal of grid voltages are estimated as follows,

$$u_{Rp} = \frac{V_{phR}}{V_T}, \quad u_{Yp} = \frac{V_{phY}}{V_T}, \quad u_{Bp} = \frac{V_{phB}}{V_T} \tag{2}$$

This article has been accepted for publication in a future issue of this journal, but has not been fully edited. Content may change prior to final publication. Citation information: DOI 10.1109/TIA.2019.2947397, IEEE Transactions on Industry Applications

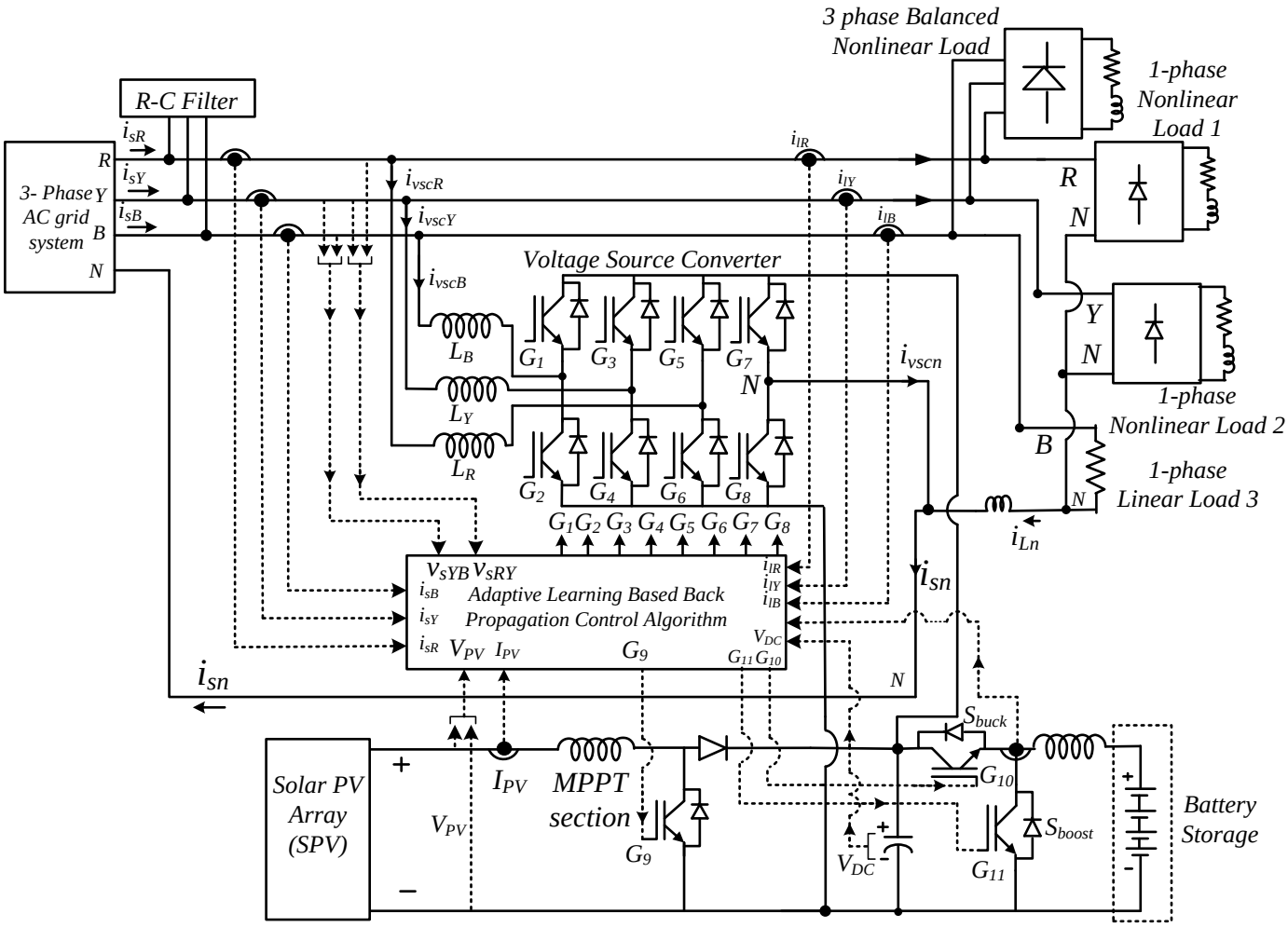

Fig.1(a) Block diagram of adaptive control of voltage source converter based scheme for grid-interactive solar PV- battery system feeding unbalanced 3 phase and single phase nonlinear and linear loads

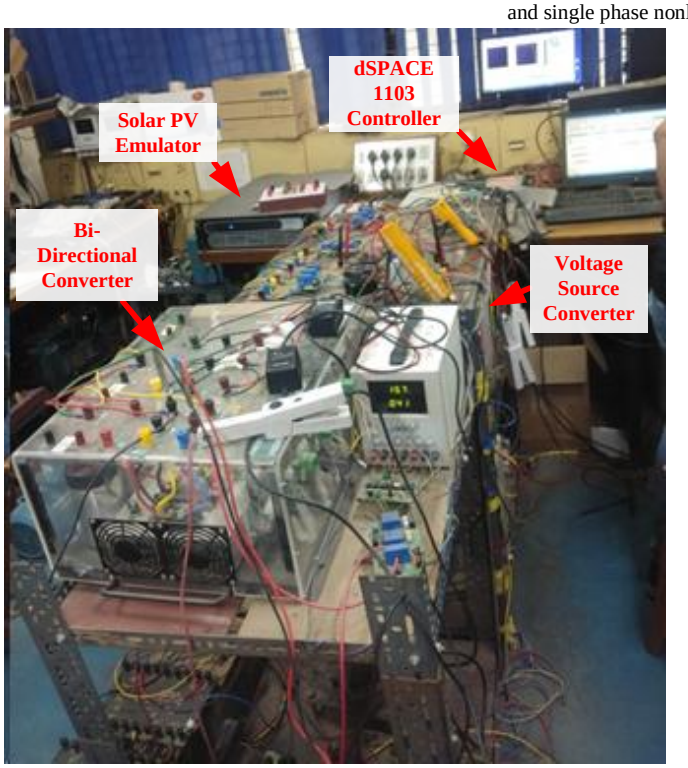

Fig. 1(b) Photograph of experimental prototype

where V_{phR}, V_{phY}, V_{phB} are phase-voltages of the grid. The quadrature normalized signals of grid-voltages are estimated as follows.

$$u_{Rq} = \frac{-u_{Yp} + u_{Bp}}{\sqrt{3}}, \quad u_{Yq} = \frac{3u_{Rp} + u_{Yp} - u_{Bp}}{2\sqrt{3}}, \quad u_{Bq} = \frac{-3u_{Rp} + u_{Yp} - u_{Bp}}{2\sqrt{3}} \tag{3}$$

An AL-BP control algorithm [27-29] estimates the weights of active-components (W_{Rp}, W_{Yp}, W_{Bp}) and reactive-components (W_{Rq}, W_{Yq}, W_{Bq}) of load currents using equations (4) to (15). The three phase nonlinear load currents i_{lR}, i_{lY}, i_{lB} are sensed using Hall Effect sensors and their measured values in each sampling interval are fed to the DSP controller (as input variables). The front end layer of AL-BP control algorithm for the fundamental component (of load current) extraction are estimated using equation (4), (5) and (6).

$$I_{lRp} = W_m + i_{lR}u_{Rp} + i_{lR}u_{Yp} + i_{lR}u_{Bp} \tag{4}$$

$$I_{lYp} = W_m + i_{lY}u_{Rp} + i_{lY}u_{Yp} + i_{lY}u_{Bp} \tag{5}$$

$$I_{lBp} = W_m + i_{lB}u_{Rp} + i_{lB}u_{Yp} + i_{lB}u_{Bp} \tag{6}$$

where W_m is initial-weight. The fundamental components of load currents I_{lRp}, I_{lYp} and I_{lBp} are processed through a sigmoid-

type activation-function using equations (7) to (9). These equations are used to estimates the outputs of feed-forward block.

$$Z_{Rp} = f\left(i_{lRp}\right) = \left(\frac{1}{1+e^{-i_{lRp}}}\right) \tag{7}$$

$$Z_{Yp} = f\left(i_{lYp}\right) = \left(\frac{1}{1+e^{-i_{lYp}}}\right) \tag{8}$$

$$Z_{Bp} = f\left(i_{lBp}\right) = \left(\frac{1}{1+e^{-i_{lBp}}}\right) \tag{9}$$

The outputs of feed-forward block (Z_{Rp}, Z_{Yp}, Z_{Bp}) are given as input to a hidden layer of back propagation neural network. The outputs of hidden layer are estimated using equations (10) to (12).

$$i_{Rp1} = W_{m1} + W_{Rp}Z_{Rp} + W_{Yp}Z_{Rp} + W_{Bp}Z_{Rp} \tag{10}$$

$$i_{Yp1} = W_{m1} + W_{Rp}Z_{Yp} + W_{Yp}Z_{Yp} + W_{Bp}Z_{Yp} \tag{11}$$

$$i_{Bp1} = W_{m1} + W_{Rp}Z_{Bp} + W_{Yp}Z_{Bp} + W_{Bp}Z_{Bp} \tag{12}$$

where W_{m1}, W_{Rp}, $W_{Yp,}$ W_{Bp} are the initial-weights of the hidden-layer. The revised value of weight of real component of phase R is estimated using equation (13),

$$W_{Rp}(k) = W_p(k) + \eta\left\{W_p(k) - W_{Rp1}(k)\right\} f'\left(i_{Rp1}\right) Z_{Rp}(k) \tag{13}$$

where $W_p(k)$ is the average weight of active power constituent of load currents, $W_{Rp}(k)$ is the revised weight value of phase R at k^{th} sampling period. $W_{Rp1}(k)$, $Z_{Rp}(k)$ are the amplitudes of fundamental weight of active power constituent of load currents of phase R and feed-forward block output at k^{th} sampling time respectively. $f'(i_{Rp1})$ is the derivative of i_{Rp1}. The η is learning rate of the proposed neural network based control scheme.

Similarly revised weights of real power constitutes of load currents of phase Y and phase B are estimated using equations (14) and (15),

$$W_{Yp}(k) = W_p(k) + \eta\left\{W_p(k) - W_{Yp1}(k)\right\} f'\left(i_{Yp1}\right) Z_{Yp}(k) \tag{14}$$

$$W_{Bp}(k) = W_p(k) + \eta\left\{W_p(k) - W_{Bp1}(k)\right\} f'\left(i_{Bp1}\right) Z_{Bp}(k) \tag{15}$$

Estimated value of i_{Rp1}, i_{Yp1}, i_{Bp1} are processed via sigmoid function, which is working as an activation function of neural network in order to estimate the fundamental real power constituents of load currents (W_{Rp1}, W_{Yp1}, W_{Bp1}) as,

$$W_{Rp1} = f\left(i_{lRp1}\right) = \left(\frac{1}{1+e^{-i_{Rp1}}}\right) \tag{16}$$

$$W_{Yp1} = f\left(i_{lYp1}\right) = \left(\frac{1}{1+e^{-i_{Yp1}}}\right) \tag{17}$$

$$W_{Bp1} = f\left(i_{lBp1}\right) = \left(\frac{1}{1+e^{-i_{Bp1}}}\right) \tag{18}$$

Average weight of fundamental real power signal (W_p) is calculated as follows,

$$W_p = \frac{W_{Rp1} + W_{Yp1} + W_{Bp1}}{3} \tag{19}$$

The output of this section is processed through a low pass filter then multiplied by scaling factor (ξ) to get final value of weight of real power component W_{lpt}.

Similarly the weights of reactive power components of load currents ($W_{q,}$ W_{Rq1}, W_{Yq1}, W_{Bq1}) are calculated and processed through a low pass filter then multiplied by scaling factor (α) to get the final value of weight of imaginary power component (W_{lqt}). Fig.2 presents the structure of control technique for DC-DC bidirectional converter for bidirectional power flow. The primary function of control algorithm is to manage the energy of battery energy storage (BES). However, the nominal voltage of the BES, is maintained throughout charging operation. The input to the PI controller is the difference between sensed DC link voltage and reference DC link voltage. The output of PI controller is the reference BES current, which is compared with the sensed battery current to originate switching sequences for bidirectional DC-DC converter. The error in system DC link voltage is estimated as,

$$V_{dcE}(k) = V_{dc}^{*}(k) - V_{dc}(k) \tag{20}$$

This voltage error is fed to the proportional-integral (PI) controller for evaluation of battery reference current.

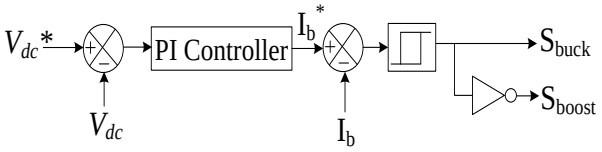

Fig.2 Control technique of bidirectional converter

The output of this PI controller is as follows.

$$I_{PL}(k) = I_{PL}(k-1) + K_{if}\left\{V_{dcE}(k) - V_{dcE}(k-1)\right\} + K_{pf}V_{dcE}(k) \tag{21}$$

where k_{pf} and k_{if} are the proportional and integral gain constants of the PI controller used in DC link voltage control loop. The magnitude of real power constituent of reference grid current (W_{Fp}) is as follows,

$$W_{Fp} = I_{PL}(k) + W_{lpt} \tag{22}$$

The magnitude of PCC voltage (V_T) is compared with its reference value (V^*_T) to calculate the error in voltage, which is processed through a PI controller as,

$$V_{TE}(k) = V_T^{*}(k) - V_T(k) \tag{23}$$

The output of this PI controller is as follows,

$$V(k) = V(k-1) + K_{iv}\left\{V_{TE}(k) - V_{TE}(k-1)\right\} + K_{pv}V_{TE}(k) \tag{24}$$

The magnitude of the imaginary power component of the reference grid currents (W_{Fq}) is calculated as follows,

$$W_{Fq} = V(k) - W_{lqt} \tag{25}$$

The real constituents of reference grid currents are calculated as follows,

$$i_{sRp} = W_{Fp}u_{Rp},\ i_{sYp} = W_{Fp}u_{Yp},\ i_{sBp} = W_{Fp}u_{Bp} \tag{26}$$

The reactive constituents of reference grid currents are calculated as follows,

$$i_{sRq} = W_{Fq}u_{Rq},\ i_{sYq} = W_{Fq}u_{Yq},\ i_{sBq} = W_{Fq}u_{Bq} \tag{27}$$

Total reference grid currents of 3 phases are calculated as follows.

$$i_{sR}^{*} = i_{sRp} + i_{sRq},\ \ i_{sY}^{*} = i_{sYp} + i_{sYq},\ \ i_{sB}^{*} = i_{sBp} + i_{sBq} \tag{28}$$

These net reference grid currents are compared with the sensed grid currents and the error of each phase current is processed through the hysteresis PWM controller in order to generate the gating pulses for the corresponding leg of the VSC.

IV. Simulated Results

Simulated performance of AL-BP control technique for grid interactive improved power quality solar PV-battery supported system is studied at the balanced and unbalanced three phase four wire (3P-4W) nonlinear loads and single phase loads of various nature simultaneously. The simulated results of AL-BP control technique based grid interactive 3-phase 4-wire system under various loading conditions, have been presented in Figs. 3 and 4. Simulated results of Fig. 3(a)-3(b), show that currents of three phases of grid are perfectly balanced, equal and sinusoidal, while the system is feeding three different types of single phase loads. These simulated results also show that harmonic current demanded by neutral of load has been fully compensated by the fourth leg of the VSC. Therefore, because of this neutral current compensation capability of the system, the neutral of the grid is not required to deliver any harmonic component of load-neutral current. These simulated results of Fig. 3(a) -3(b), also show that the shape of current of VSC in all three phases are different in order to maintain equal and balanced three phase currents at grid side while the system is feeding unequal currents in different phases of the load. Fig. 3(c) show the waveforms and THDs of the grid currents. Fig. 3(d) show the waveforms and THDs of load currents. Simulated results of Fig. 3(c)-3(d) show that the THD in grid current is less than 5%. Therefore the proposed system is confirming the IEEE 519 standard. Fig.4 shows the performance of the system under critically unbalanced system while the load of one of the phase is disconnected and remaining two phases are feeding 1-phase linear and nonlinear loads respectively.

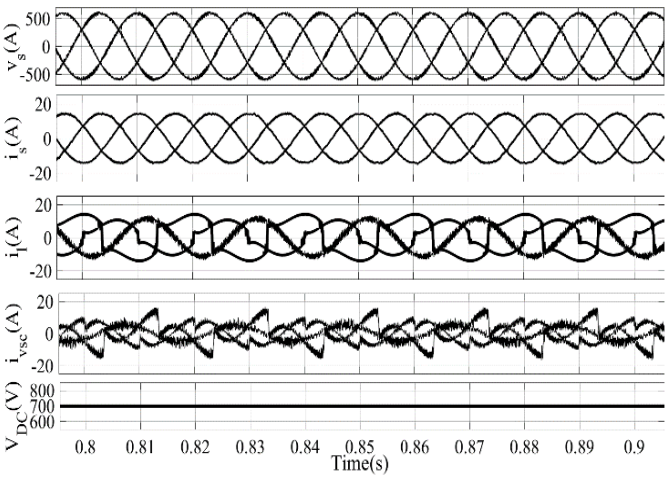

Fig. 3 (a) Grid voltages (v_s), Grid currents (i_s), Load currents (i_l), VSC currents (i_{vsc}) and DC link voltage (V_{DC})

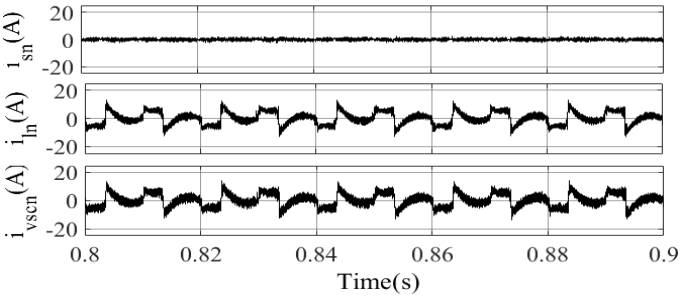

Fig. 3 (b) Load -Neutral current (i_{ln}), Grid-Neutral current (i_{sn}), VSC-Neutral current (i_{vscn})

Fig. 3(a)-3(b) Steady state simulated performance of the proposed 3 phase 4 wire grid integrated solar PV - battery system feeding unbalanced 3 phase and single phase nonlinear and linear loads.

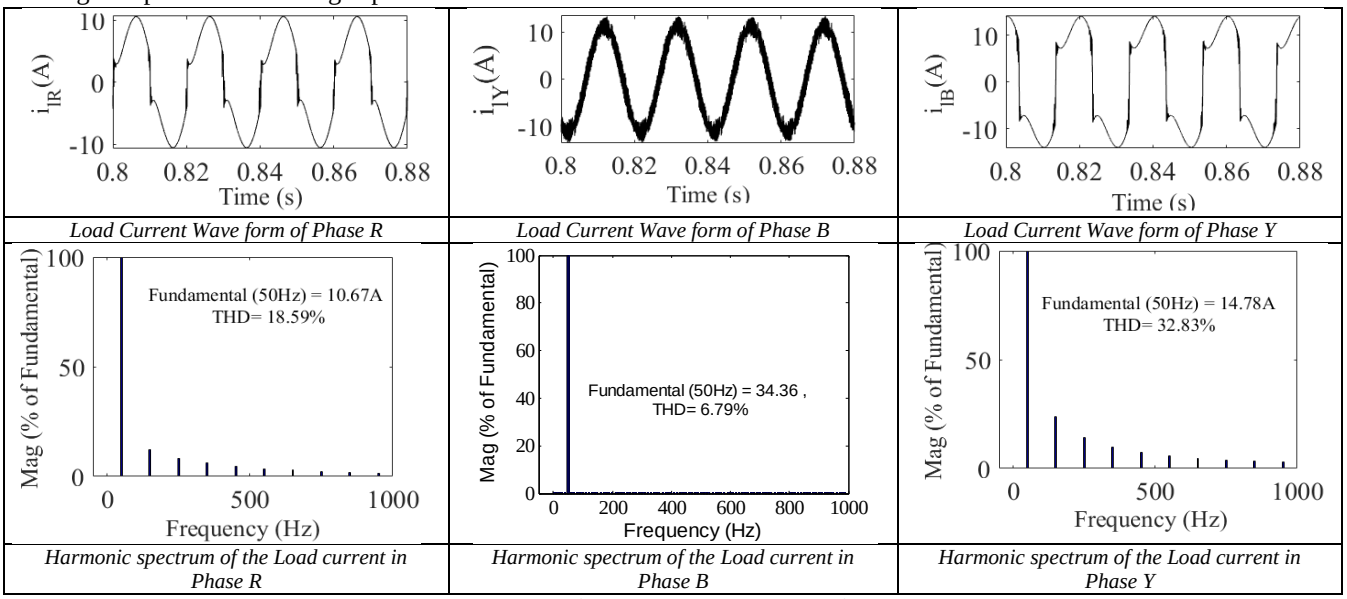

Fig. 3 (c) Simulated waveform and harmonic spectrum of the grid currents

This article has been accepted for publication in a future issue of this journal, but has not been fully edited. Content may change prior to final publication. Citation information: DOI 10.1109/TIA.2019.2947397, IEEE Transactions on Industry Applications

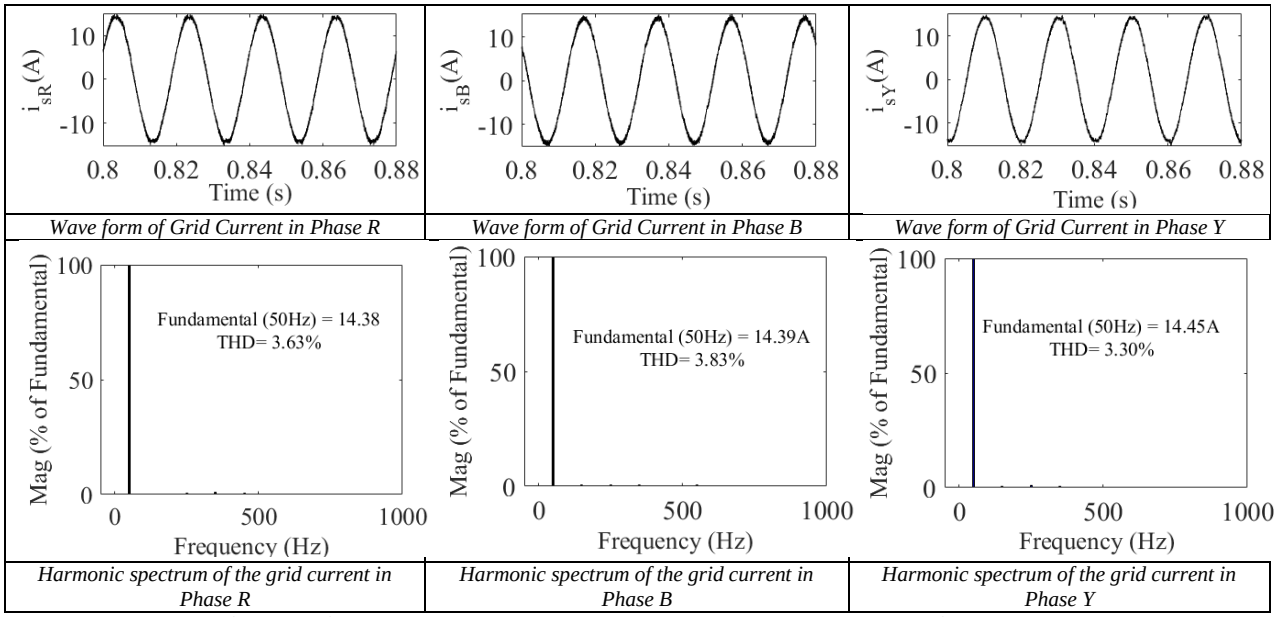

Fig. 3(d) Simulated performance of the proposed 3 phase 4 wire grid interactive solar PV - battery system feeding unbalanced 3 phase and single phase nonlinear and linear loads

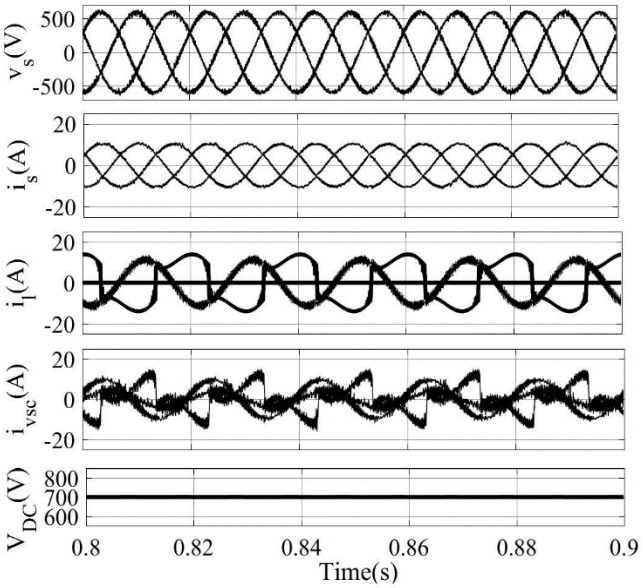

Fig 4(a) Grid voltages (v_s), Grid currents (i_s), Load currents (i_l), VSC currents (i_{vsc}) and DC link voltage (V_{DC})

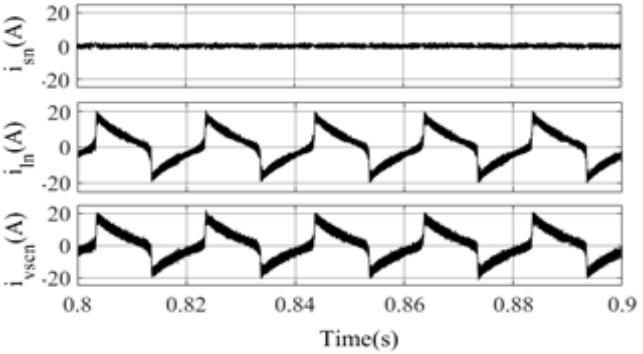

Fig 4(b) Load -Neutral current (i_{ln}), Grid-Neutral current (i_{sn}), VSC-Neutral current (i_{vscn})

Fig. 4 Simulated performance of interactive solar PV - battery system feeding unbalanced 3 phase and single phase nonlinear and linear loads

This simulated result confirms that the grid side current in all three phases are balanced, equal and sinusoidal under critically unbalanced loading conditions. In such critically unbalanced loading conditions, the neutral of the load demands highly non sinusoidal current of almost triangular shape, which is fully compensated by the fourth leg of VSC, therefore no harmonic current component of the neutral of load are required to be delivered by the grid. These simulated results indicate 32.83% THD of the current drawn by this single phase nonlinear load, whereas THD of grid current in same phase is less than 5%, therefore system is meeting IEEE 519 standard.

V. Experimental Results and Discussion

The proposed scheme has been implemented using a DSP based controller (dSPACE 1103) in real time. The DSP controller requires minimum sampling time of 30 µs to execute the proposed control algorithm. This section includes the experimental performances of proposed AL-BP Algorithm for battery supported three phase four wire (3P4W) system feeding various linear and nonlinear loads.

A. Steady State Behavior at Three Phase Four Wire Load and Battery Charging Conditions

Fig. 5 presents experimental results under balanced nonlinear loads and battery charging conditions. The i_{sR} is sinusoidal however, i_{lR} is nonlinear in nature as depicted in Figs. 5(a)-(b). The net power drawn from the PV string is injected to VSC and battery energy storage as illustrated in Fig. 5(c) and then distributed to the grid and loads. The grid neutral current *(i_{sn})*, load neutral current *(i_{ln})* and VSC neutral current *(i_{vscn})* are shown in Figs. 5(d)-(f). The magnitude of i_{sn} is 0.642 A as the effect of i_{ln} is eliminated by fourth leg of the VSC. Therefore, VSC supplies exact magnitude of i_{vscn} which is needed to compensate i_{ln}. Figs. 5(g)-(i) show the active and

reactive powers injected to 3P4W distribution network, load power and VSC power. The net active power fed to the distribution system is 2.77 kW and reactive power is zero and unity power factor operation is depicted in Fig. 5(g). The power absorbed by the load is 1.16 kW. Hence, the power coming from VSC is (2.77kW+1.16kW=3.93kW), which is depicted in Fig. 5(i). Moreover, reactive power required by nonlinear load is injected by 4-leg VSC. Figs. 5(j)-(k) show the load current and grid current THDs, which are 30.6 % and 2.2 % and well within the IEEE-519 standard. Besides, the power fed to the grid, the battery charging state is also included in Fig. 5 (l). The battery current is negative, which means battery is in changing state when it is needed otherwise it is to be in floating mode.

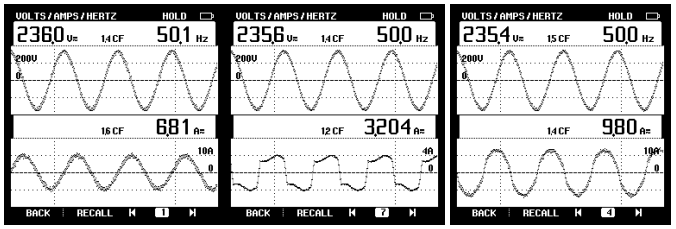

Fig. 5(a) V_{sR},i_{sR}

Fig. 5(b) V_{lR},i_{lR}

Fig. 5(c) V_{vscR},i_{vscR}

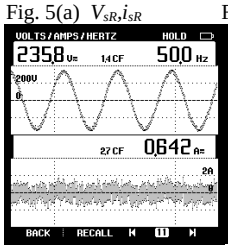

Fig. 5(d) i_{sn}

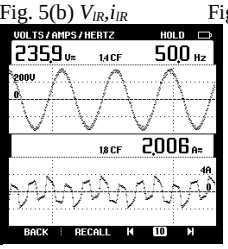

Fig. 5(e) i_{ln}

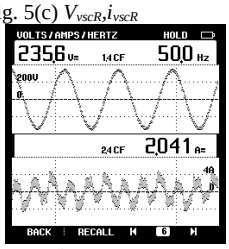

Fig. 5(f) i_{vscn}

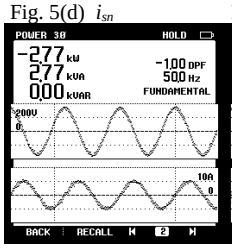

Fig.5(g) Grid Power

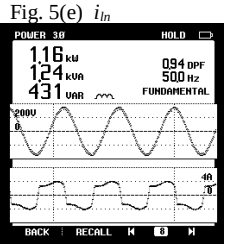

Fig. 5(h) Load Power

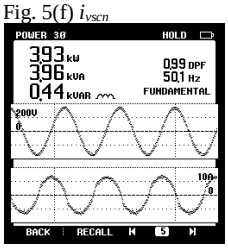

Fig. 5 (i) VSC Power

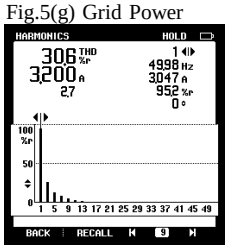

Fig. 5 (j) THD in i_{lR}

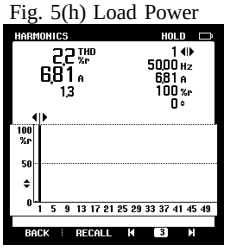

Fig. 5 (k) THD in i_{sR}

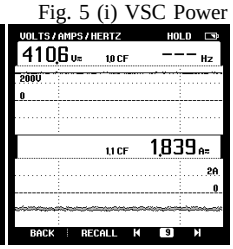

Fig. 5 (l) V_{batt} & i_{batt}

Fig. 5 Test results under balanced nonlinear loads (a)-(c) v_{sRY} with i_{sR}, i_{lR}, $i_{VSCR,}$ (d)-(f) v_{sRY} with $i_{sn,}$, i_{vscn} and $i_{ln,}$ (g)-(i) Grid power, load power and VSC power, (j)-(l) Harmonic spectrum of (i_{lR}), (i_{sR}) and battery voltage and current in charging Mode

B. Steady State Behaviour of System at Unbalanced Load

In real time operational conditions of 3-phase 4-wire system, the amount of load on different phases are always different at various level of nonlinearity, since the different single phase loads are always of varying power levels. The different single phase loads connected in all three phases demands varying amount of active and reactive powers are having varying power factor. The proposed scheme is tested under all these practical unbalance loading conditions, which may be verified using Figs. 6(a) to 6(i) of test results. The proposed system is found to be highly balanced in such critically unbalanced and nonlinear loading conditions. Moreover it also meets the IEEE 519 standard of power quality. The THDs in currents of all three phases are found to be less than 5%. Fig. 6 shows test results of proposed 3-phase 4 wire system under unbalanced loading condition. The unbalancing in the system is appeared because of two nonlinear single phase loads of different values are connected in phase *R* and in phase *Y*, respectively. A single phase linear load is connected in phase *B*. The battery is kept in floating mode of operation. Figs. 6(a), 6(b) and 6(c) show the waveforms of grid voltages and load currents in the phases *R*, *Y* and *B* respectively. These test results show that two single phase nonlinear loads of different values are connected in phase *R* and *Y*, respectively, which are drawing almost square wave current and a linear load is connected at phase B which is drawing sinusoidal current. Figs. 6(d)-6(f) show that all three single phase loads connected in phase *R*,*Y* and *B*, respectively, are of different values and drawing currents of different THD values, therefore it causing a significant unbalance in the proposed 3 phase 4 wire system. Figs. 6(g)-6(i) depict the harmonic spectrum and THD in load currents of phases *R*, *Y* and *B* respectively, which shows that the nonlinearity and THD in load current of each phase are significantly different in proposed system under test. Figs. 6(a)-6(i) show that the proposed system is tested under highly unbalanced conditions. The THDs in nonlinear load currents of phase *R* & *Y* are very high of the order of 35.4% and 42.4% respectively and THD in linear load current in phase *B* is of the order of 2%. Figs. 6(j)-6(l) show that the grid currents in three phases are found to be almost equal, truly sinusoidal and balanced, whereas the load currents in each of three phases are of different values and having different level of nonlinearity. Figs. 6(m)-6(o) are showing that an almost equal power is being fed into the grid through each phase from solar PV array which shows that proposed controller is maintaining balanced currents at grid side in all three phases while the system is feeding highly unbalanced 3 phase loads. Figs. 6(p)-6(r) show the harmonic spectrum of grid currents in phases *R*,*Y* and *B* respectively. The THD in grid current of every phase are found to be less than 5%. Therefore, proposed system is meeting the IEEE 519 standard of the power quality that proves the harmonic mitigation and power quality improvement capabilities of the system. Figs. 6(s)-6(u) present the recorded waveforms of VSC currents and voltages in phases *R*, *Y* and *B*, respectively. The VSC is having different shapes of currents in each of three phases in order to obtain balance currents and power at grid side under unbalanced loading conditions. Figs. 6(v) to 6(x) show that the VSC adjust the shape of currents in different phases in order to inject a balanced and equal active and reactive powers in all three phases in grid side while system is catering an unequal loads in different phases. Figs. 6(y)-6(z_1) show that VSC is supplying currents of different harmonics and THD in different phases in order to compensate the harmonic currents of injected by unbalanced 3 phase nonlinear loads in proposed system.

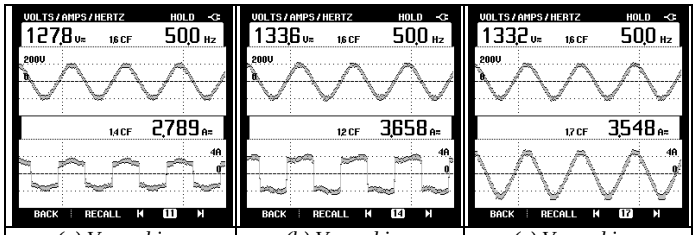

(a) V_{sR} and i_{lR}

(b) V_{sY} and i_{lY}

(c) V_{sB} and i_{lB}

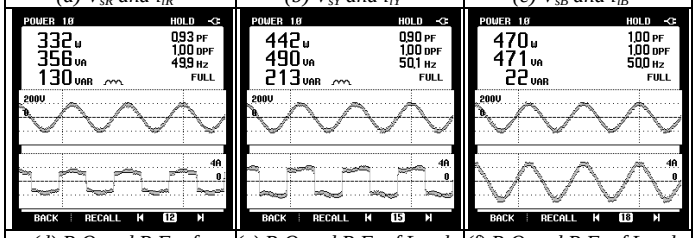

(d) P,Q and P.F. of Load in phase R

(e) P,Q and P.F. of Load in phase Y

(f) P,Q and P.F. of Load in phase B

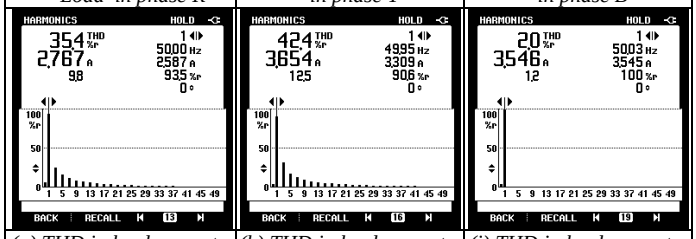

(g) THD in load current of Phase R

(h) THD in load current of Phase Y

(i) THD in load current of Phase B

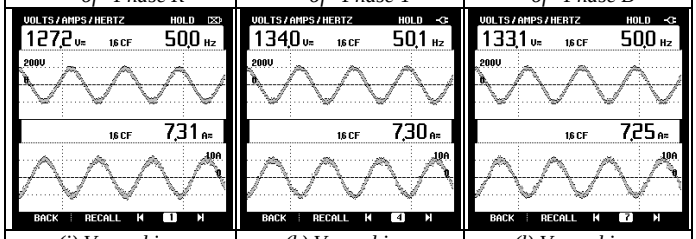

(j) V_{sR} and i_{sR}

(k) V_{sY} and i_{sY}

(l) V_{sB} and i_{sB}

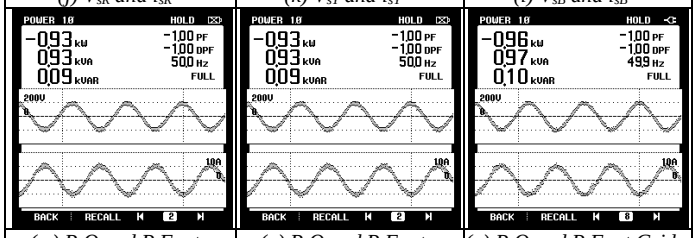

(m) P,Q and P.F. at Grid in phase R

(n) P,Q and P.F. at Grid in phaseY

(o) P,Q and P.F. at Grid in phase B

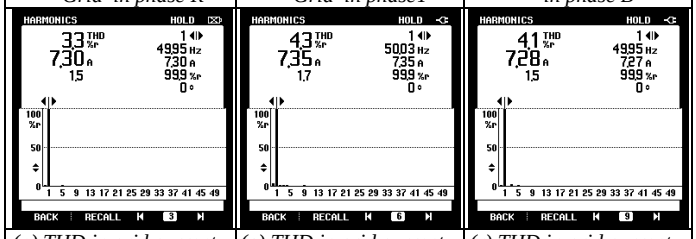

(p) THD in grid current of Phase R

(q) THD in grid current of Phase Y

(r) THD in grid current of Phase B

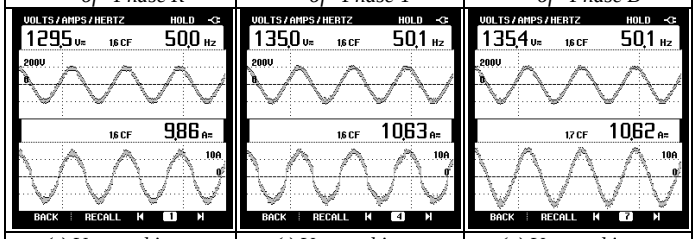

(s) V_{vscR} and i_{vscR}

(t) V_{vscY} and i_{vscY}

(u) V_{vscB} and i_{vscB}

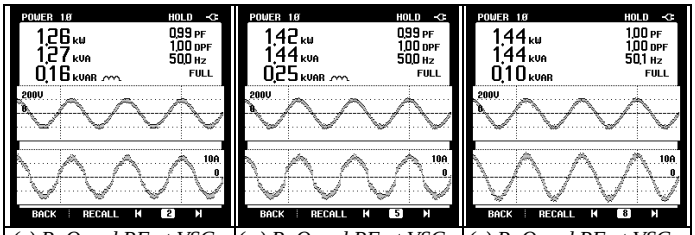

(v) P, Q and PF at VSC side in phase R

(w) P, Q and PF at VSC side in phase Y

(x) P, Q and PF at VSC side in phase B

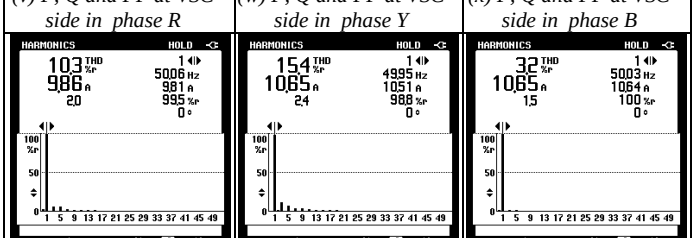

(y) Harmonic spectrum of i_{vscR}

(z)) Harmonic spectrum of i_{vscY}

(z_1)) Harmonic spectrum of i_{vscB}

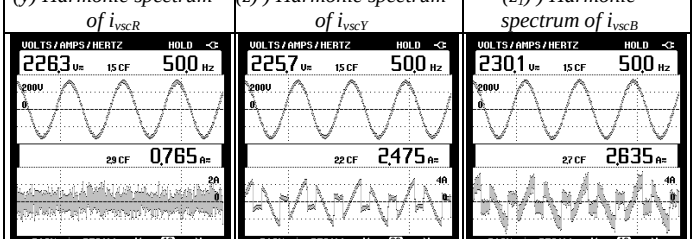

(z_2) neutral current at grid side

(z_3) neutral current at load side

(z_4) neutral current at VSC side

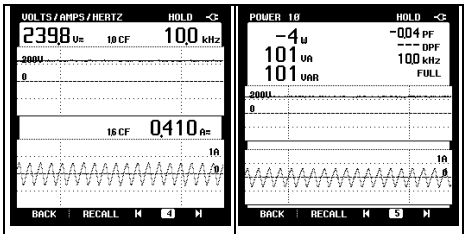

(z_5) V_{batt} & i_{batt} | (z_6) power Transaction through battery

Fig 6. Test results of the proposed system under significantly unbalanced 3-phase 4 wire loading conditions

Figs. 6(z_2)-6(z_4) show the neutral currents at grid side, load side and VSC side respectively. Because of the unbalanced and nonlinear loading conditions, a large amount of harmonics currents are demanded by the neutral of unbalanced 3-phase 4 wire system feeding different nonlinear and linear loads. All the harmonic currents demanded by the load neutral are compensated and supplied by the VSC in the proposed 3-phase 4 wire system as shown by Figs. 6(z_2)-6(z_4). Figs. 6(z_5)-6(z_6) show the battery current, voltage and power transaction through battery under floating mode of operation.

C. Steady State Behaviour of System at Critically Unbalanced Load

Fig. 7 show test results and response of the system under critically unbalanced 3-phase 4-wire load. A critical unbalance caused by the disconnection of the load in phase *R* as shown in Fig.7(a) and a highly nonlinear load is connected in phase *Y*, which is drawing almost square wave current as shown in Fig. 7(b). A single phase linear load is connected in phase *B*, which is drawing sinusoidal current as shown in Fig. 7(c).

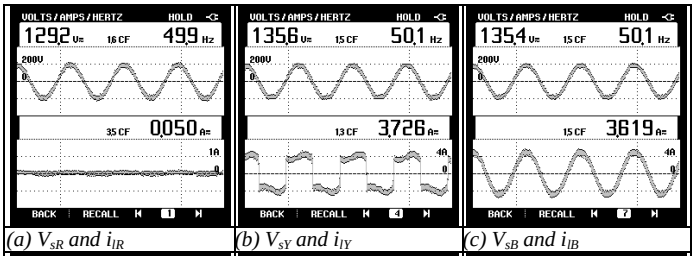

(a) V_{sR} and i_{lR} (b) V_{sY} and i_{lY} (c) V_{sB} and i_{lB}

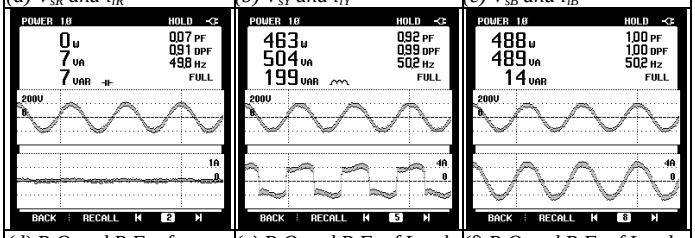

(d) P,Q and P.F. of Load in phase R (e) P,Q and P.F. of Load in phase Y (f) P,Q and P.F. of Load in phase B

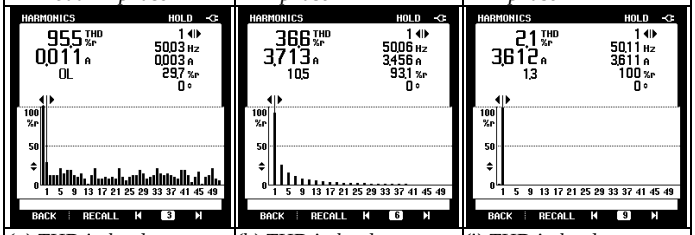

(g) THD in load current of Phase R (h) THD in load current of Phase Y (i) THD in load current of Phase B

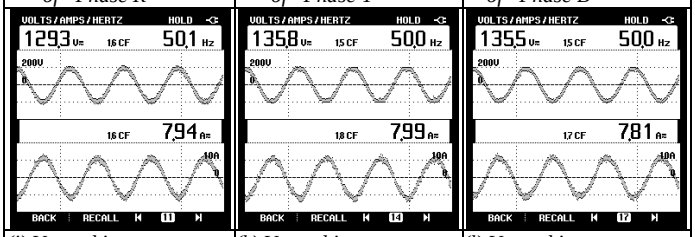

(j) V_{sR} and i_{sR} (k) V_{sY} and i_{sY} (l) V_{sB} and i_{sB}

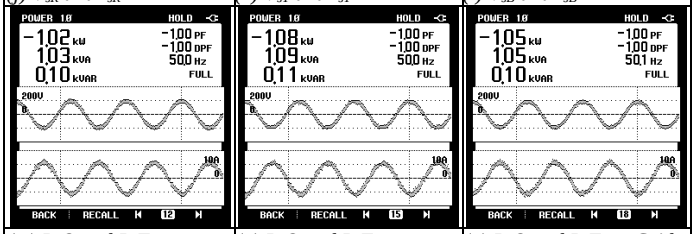

(m) P,Q and P.F. at Grid in phase R (n) P,Q and P.F. at Grid in phaseY (o) P,Q and P.F. at Grid in phase B

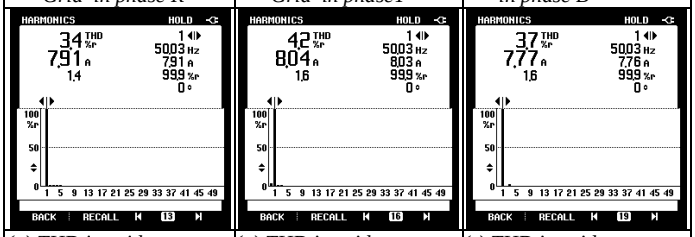

(p) THD in grid current of Phase R (q) THD in grid current of Phase Y (r) THD in grid current of Phase B

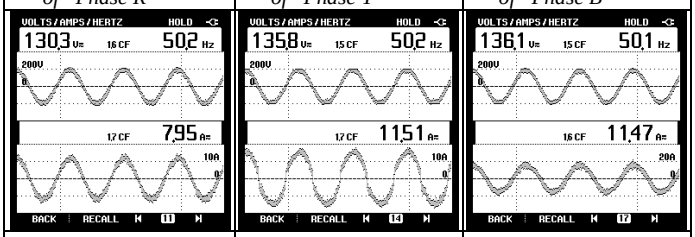

(s) V_{vscR} and i_{vscR} (t) V_{vscY} and i_{vscY} (u) V_{vscB} and i_{vscB}

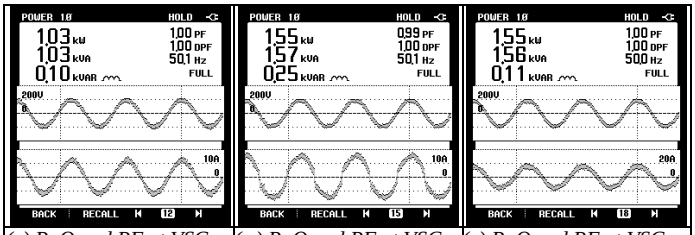

(v) P, Q and PF at VSC side in phase R (w) P, Q and PF at VSC side in phase Y (x) P, Q and PF at VSC side in phase B

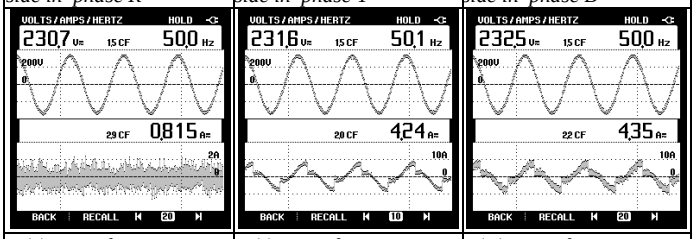

(y) neutral current at grid side (z) neutral current at load side (z_1) neutral current at VSC side

Fig 7. Test results of system at critically unbalanced 3-phase 4 wire loading conditions

This is one of the most critical kind of unbalanced condition, which may appear at severe abnormal conditions. The system is found to be perfectly balanced under such critical unbalanced loading. Figs. 7(j)-7(l) and Figs. 7(p)- 7(r) show that grid current in all three phases remain equal and perfectly sinusoidal with THD in source currents of less than 5%. Therefore proposed system is meeting the IEEE 519 standard of power quality. Figs. 7(m)-7(o) show that the amount of power injected into each phase of the grid is also found to be equal under such critically unbalanced loading conditions. Figs. 7(s) - 7(u) show that the VSC currents in phases *R*, *Y* and *B* respectively. The test results of Fig 7 show that the 4 leg VSC adjusts the shape and magnitude of currents to operate 3-phase 4-wire system as a balanced system while feeding critically unbalanced loads. Figs. 7(v) to 7(x) show the reactive and active power transaction made through VSC in phases *R*, *Y* and *B* respectively. Fig. 7(y) shows the neutral current drawn by the system from the grid. Fig. 7(z) shows the neutral current demanded by load. Fig. 7(z_1) shows the neutral current fed by the fourth leg of VSC which shows that all the harmonic currents demanded by the neutral of the unbalanced load have been compensated by the fourth leg of VSC and there is no component of neutral current drawn from the grid which reduces the losses and improves the system power quality.

D. Dynamic Behavior Under Three Phase Four wire Load and Battery Charging Conditions

Test results shown in Fig. 8(a), present four signals (from top to bottom) namely solar PV current (channel 1), sudden change in load current in phase *R* (channel 2), source current in phase *R* (channel 3) and VSC current in phase *R* (channel 4). Figs. 8(b) shows (from top to bottom) the load current in phase *R* (channel 1) and the channels 2, 3 and 4 show the grid side currents in phases *R*, *Y* and *B*, respectively. Figs. 8(a)-8(b) show that the sudden removal of load in phase *R* does not affect the shape and magnitude of current in respective phase or in any other phase at grid side. Therefore, the proposed system is found to be stable in this dynamic loading condition in real time.

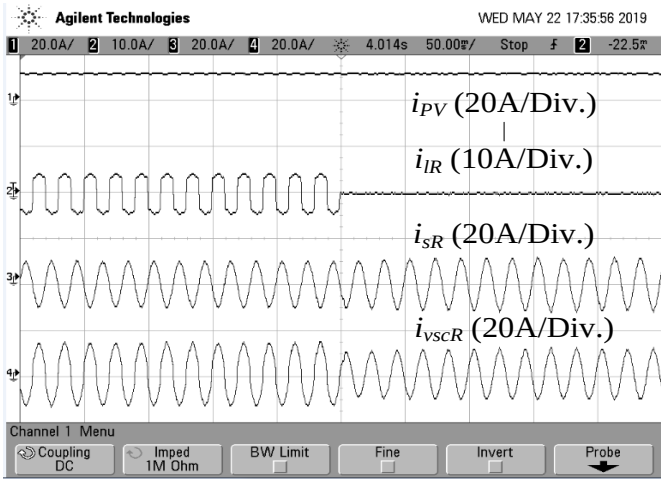

Fig. 8(a) Effect of change in load current (R Phase) on I_{pv}, i_{lR}, i_{sR} and i_{vscR}

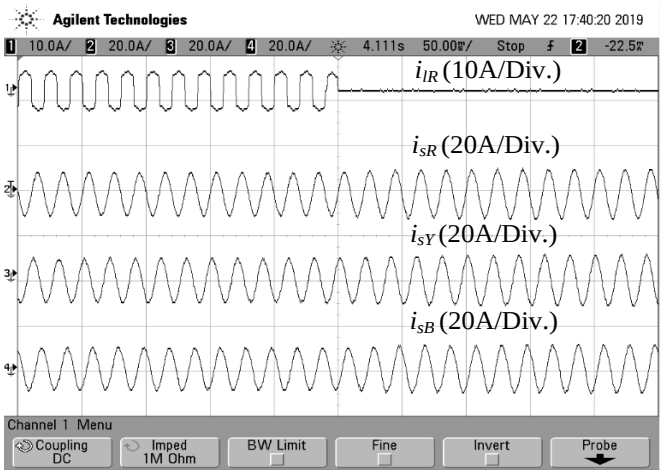

Fig. 8(b) Effect of sudden loss of Load in R Phase on i_{lR}, i_{sR}, i_{sY} and i_{sB}

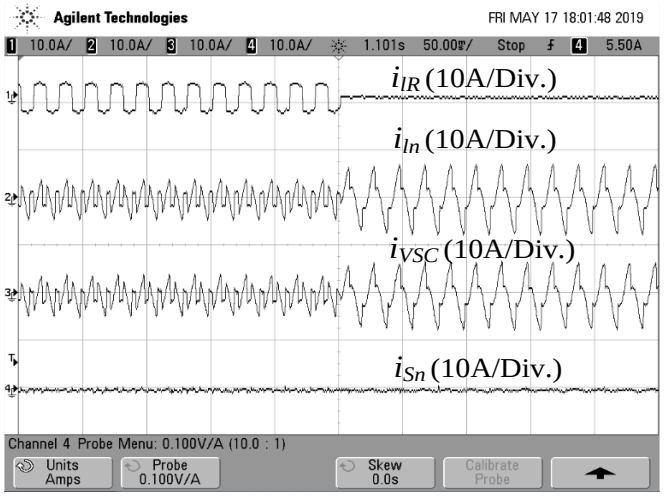

Fig. 8 (c) Effect of loss of load in R Phase on i_{lR}, i_{Ln}, i_{VSC} and i_{sn}

Fig. 8 (c) shows the effect of sudden removal of load in *R* Phase on i_{lR}, i_{ln}, i_{VSC} and i_{sn}.. Figs.9 (a)-(c) present test results under sudden increase of nonlinear loads of phase *R* and PV parameters and battery charging conditions are shown in Fig. 9 (d). Fig. 9(a) presents load currents (i_{lR}, i_{lY}, i_{lB}) and DC voltage (V_{dc}) at load change by closing of phase *R*. Under load perturbation condition, DC link voltage remains constant. Fig. 9(b) illustrates the v_{sR} of phase *R*, neutral load current *(i_{ln})*,neutral VSC current *(i_{vscn})* and grid neutral current *(i_{sn})* at connection of loads. The i_{ln} is large under unbalanced load, which is compensated by the *(i_{vscn})*. Whereas, grid neutral current is sustained to its original (zero) value under perturbation of loads. Fig. 9(c) presents unit templates *(u_{Rp}, u_{Rq})* obtained from the grid voltage *(v_{sR})* and in grid current*(i_{sR}) and* grid reference current*(i_{sR}*)*. Under load perturbation, it is observed that the grid current is increased under reduction of load power. However, the change is not noticed in unit templates. The response under battery charging condition is shown in Fig. 9(d). The power generated from the PV array is constant as no change is observed in the PV voltage and current.

E. Behavior of PV-Battery System at Change in Insolation

Figs. 10(a)-(b) and Figs. 10(c)-(d) present the response of PV-battery system under sudden decrease and increase in insolation. The PV voltage *(V_{pv})*,the change in DC link voltage *(V_{dc})*, PV current *(I_{pv})*, and extracted PV power *(P_{pv})*are illustrated in Fig. 10(a) at a decrease in insolation from 1000 W/m^2 to 500 W/m^2, V_{dc} stands to its actual magnitude, i_{sR}, I_{vscR}, I_{batt} and i_{lR} are illustrated in Fig. 10(b) at reduction in insolation.

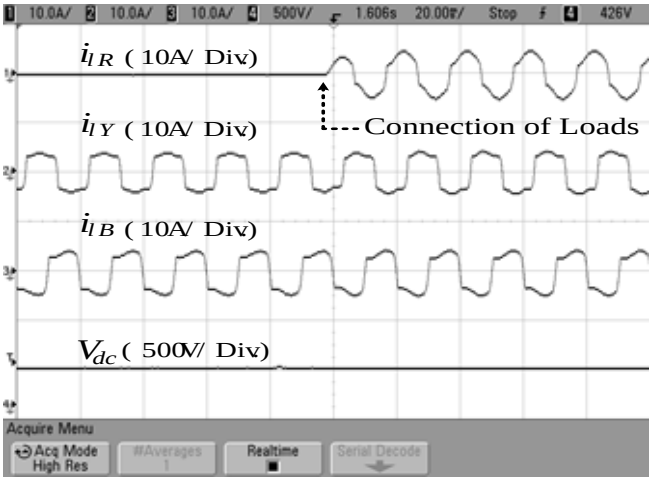

Fig. 9(a) Effect of sudden connection of load on DC bus voltage

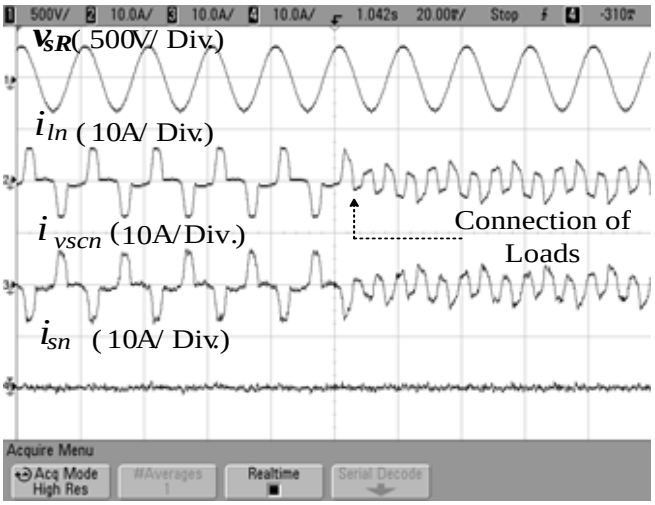

Fig. 9(b) Effect of sudden connection of load on load neutral current (i_{ln}), VSC neutral current (i_{vscn}) and source neutral current (i_{sn})

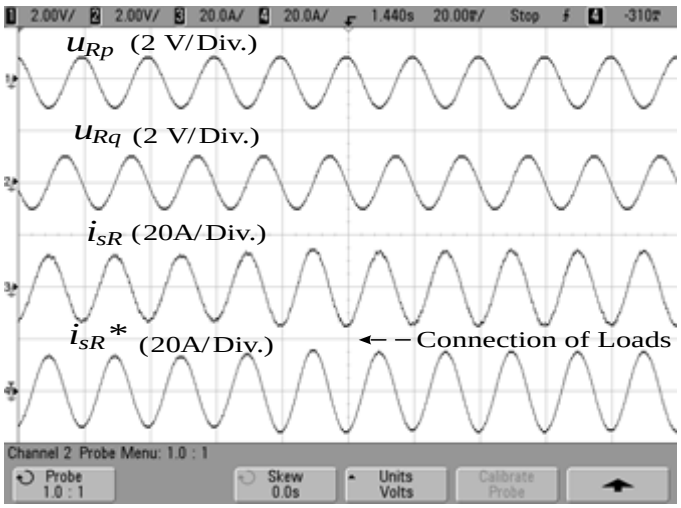

Fig. 9(c) Effect of connection of load on unit templates

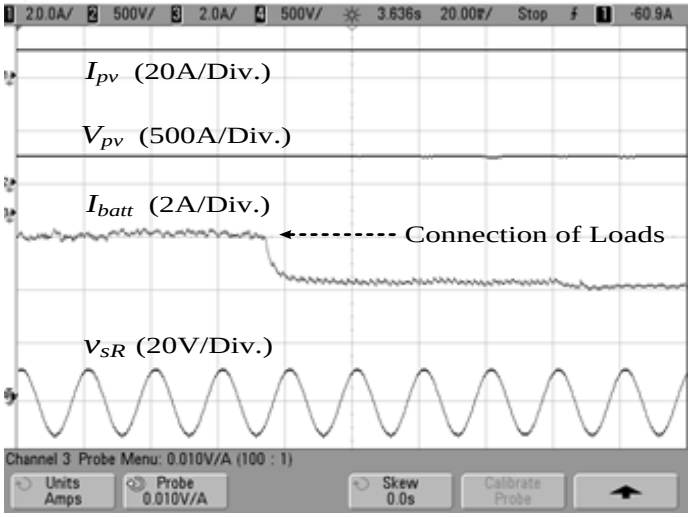

Fig. 9(d) Effect of connection of load on battery charging

Fig. 9 (a)-(c) Dynamic system performance under varying load condition, (d) Dynamic system performance under battery charging condition

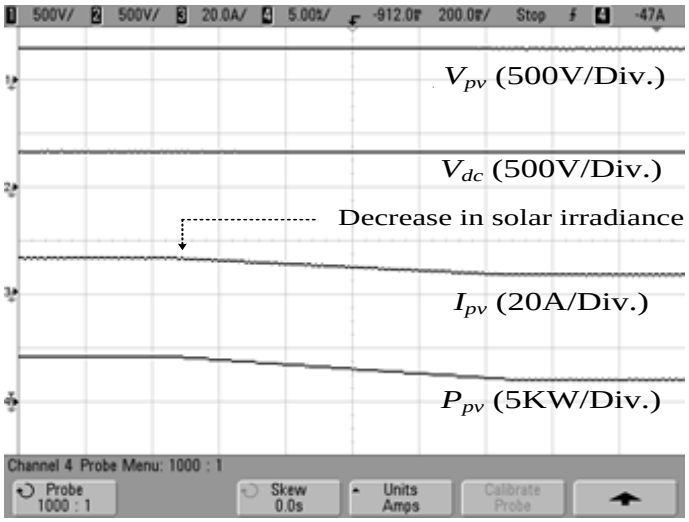

Fig. 10(a) Effect of sudden decrease in insolation on PV battery system

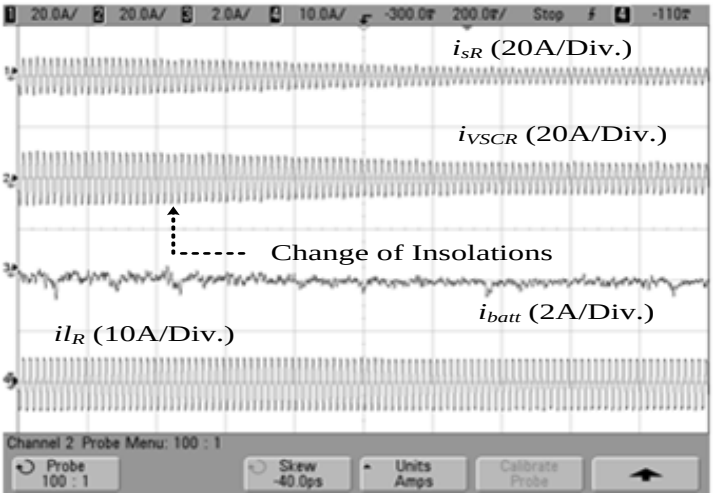

Fig. 10(b) Effect of sudden decrease in insolation on source current and battery current

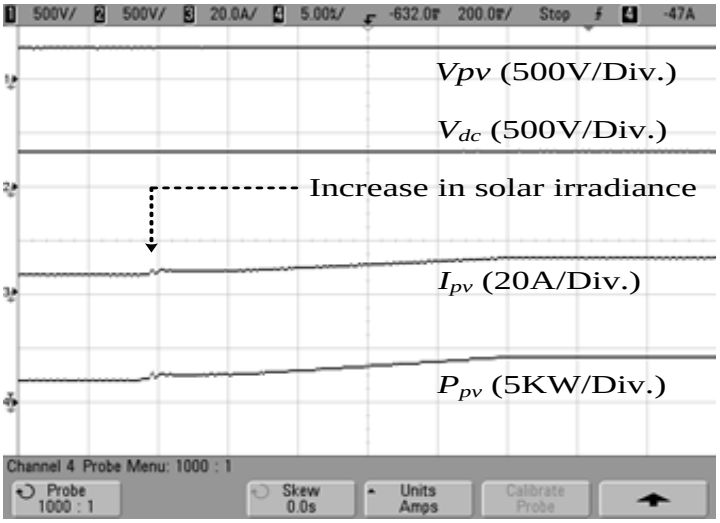

Fig. 10(c) Effect of sudden increase in insolation on PV battery systems

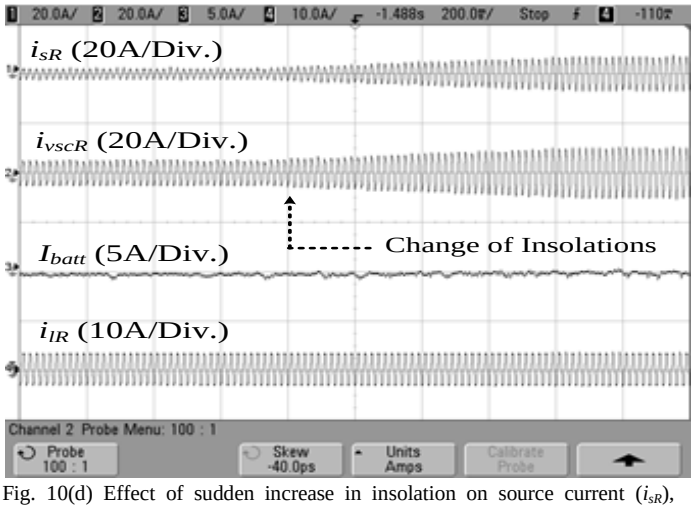

Fig. 10(d) Effect of sudden increase in insolation on source current (i_{sR}), battery current (I_{batt}) and load current (i_{lR})

Fig. 10 Dynamic system performance under varying insolation level

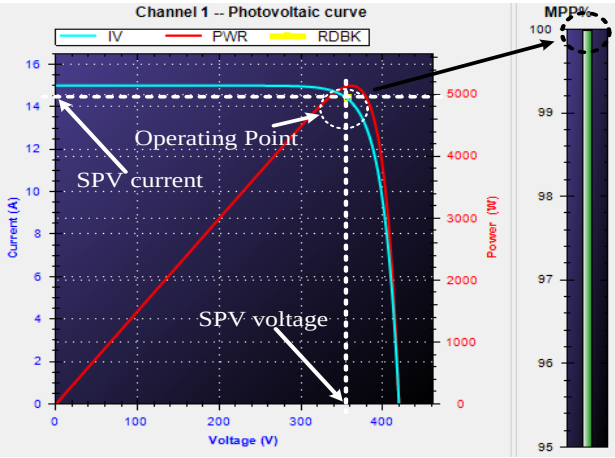

Fig. 11 MPPT tracking performance of the solar PV system

The required variation is noticed in grid current. In this condition, the battery is in floating mode as the power fed to the grid is not limited. Therefore, all the surplus power from the solar besides the load is supplied to the grid. A vice-versa effect is observed in Figs. 10 (c)-(d). Fig. 11 illustrates the satisfactory MPPT tracking response of PV battery system at 1000 W/m^2. This curve shows that the MPPT (Maximum Power Point Tracking) percentage is near to 100 % as the operating point is at its MPP (Maximum Power Point). However, the step size of the MPPT algorithm decides the steady state oscillations and dynamic response tracking.

VI. Assessment of Proposed Control With Conventional Controllers

Fig. 12 shows the comparative evaluation of proposed AL-BP control technique for grid interactive improved power quality solar PV-battery supported 3P-4W system with conventional control techniques under sudden application of load in phase *R*.

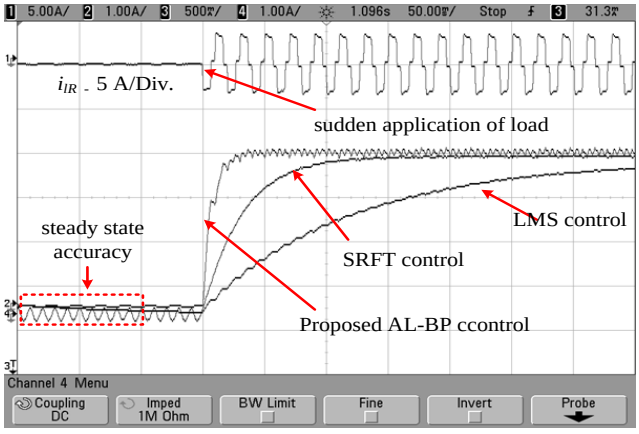

Fig. 12 Comparison of proposed adaptive cotrol with conventional techniques

In this dynamic loading condition, it is found that the proposed control technique has faster dynamic response than the conventional control schemes. The fundamental component of load current has been settled at its new revised value in less time as compared to the conventional control techniques. Moreover, the steady state and dynamic responses controlling factors are also found larger in conventional control algorithms as compared to proposed AL-BP based control technique.

VII. Conclusion

The implementation of an AL-BP control technique for grid interactive improved power quality solar PV-battery supported system catering the balanced and unbalanced three phase four wire (3P-4W) nonlinear loads and single phase loads of various nature simultaneously has been successfully presented in this work. Experimental and simulated performances of the AL-BP control technique for grid interactive improved power quality solar PV-battery supported system have shows that the proposed scheme is found capable of catering the balanced and unbalanced three phase four wire (3P-4W) nonlinear loads and single phase loads of various nature simultaneously. Moreover, the source currents have also been found balanced and sinusoidal for all operating and loading conditions such as in highly unbalance loading conditions where load on one of the phase is disconnected. The proposed system is meeting the IEEE standard of power quality.

Acknowledgments

The authors are highly thankful of SERB DST, Govt. of India, for supporting this project under Grant Number: EMR/2017/000014.

References

[1] *Basic* F. -. Chen, "Back-propagation neural networks for nonlinear self-tuning adaptive control," *IEEE Control Systems Magazine*, vol. 10, no. 3, pp. 44-48, April 1990.

[2] S. Siu, Ching-Haur Chang and Che-Ho Wei, "L/sub p/ norm back propagation algorithm for adaptive equalization," *IEEE Transactions on Circuits and Systems II: Analog and Digital Signal Processing*, vol. 42, no. 9, pp. 604-607, Sept. 1995.

[3] C. -. Hsu, M. -. Kang and C. -. Chen, "Design of adaptive load shedding by artificial neural networks," *IEE Proceedings - Generation, Transmission and Distribution*, vol. 152, no. 3, pp. 415-421, 6 May 2005

[4] Hsi-Chin Hsin, Ching-Chung Li, Mingui Sun and R. J. Sclabassi, "An adaptive training algorithm for back-propagation neural networks," *IEEE Transactions on Systems, Man, and Cybernetics*, vol. 25, no. 3, pp. 512-514, March 1995.

[5] P. Zhao and O. P. Malik, "Design of an Adaptive PSS Based on Recurrent Adaptive Control Theory," *IEEE Transactions on Energy Conversion*, vol. 24, no. 4, pp. 884-892, Dec. 2009.

[6] P. Wei, C. Cheng and T. Liu, "A Photonic Transducer-Based Optical Current Sensor Using Back-Propagation Neural Network," *IEEE Photonics Technology Letters*, vol. 28, no. 14, pp. 1513-1516, 15 July15, 2016.

[7] L. Jin, P. N. Nikiforuk and M. M. Gupta, "Direct adaptive output tracking control using multilayered neural networks," *IEE Proceedings D - Control Theory and Applications*, vol. 140, no. 6, pp. 393-398, Nov. 1993.

[8] T. Jain, S. N. Singh and S. C. Srivastava, "Adaptive wavelet neural network-based fast dynamic available transfer capability determination," *IET Generation, Transmission & Distribution*, vol. 4, no. 4, pp. 519-529, April 2010.

[9] M. Saerens and A. Soquet, "Neural controller based on back-propagation algorithm," *IEE Proceedings F - Radar and Signal Processing*, vol. 138, no. 1, pp. 55-62, Feb. 1991.

[10] S. Cong and Y. Liang, "PID-Like Neural Network Nonlinear Adaptive Control for Uncertain Multivariable Motion Control Systems," *IEEE Transactions on Industrial Electronics*, vol. 56, no. 10, pp. 3872-3879, Oct. 2009.

[11] R. C. Frye, E. A. Rietman and C. C. Wong, "Back-propagation learning and nonidealities in analog neural network hardware," *IEEE Transactions on Neural Networks*, vol. 2, no. 1, pp. 110-117, Jan. 1991.

[12] W. Ding and D. Liang, "Modeling of a 6/4 Switched Reluctance Motor Using Adaptive Neural Fuzzy Inference System," *IEEE Transactions on Magnetics*, vol. 44, no. 7, pp. 1796-1804, July 2008.

[13] P. J. Antsaklis, "Neural networks for control systems," *IEEE Transactions on Neural Networks*, vol. 1, no. 2, pp. 242-244, June 1990.

[14] F. D. Zahlay, K. S. Rama Rao and T. B. Ibrahim, "A New Intelligent Autoreclosing Scheme Using Artificial Neural Network and Taguchi's Methodology," *IEEE Transactions on Industry Applications*, vol. 47, no. 1, pp. 306-313, Jan.-Feb. 2011.

[15] P. Shamsollahi and O. P. Malik, "Direct neural adaptive control applied to synchronous generator," *IEEE Transactions on Energy Conversion*, vol. 14, no. 4, pp. 1341-1346, Dec. 1999.

[16] J. Sztipanovits, "Dynamic backpropagation algorithm for neural network controlled resonator-bank architecture," *IEEE Transactions on Circuits and Systems II: Analog and Digital Signal Processing*, vol. 39, no. 2, pp. 99-108, Feb. 1992.

[17] Li-Min Du, Zi-Qiang Hou and Qi-Hu Li, "Optimum block-adaptive learning algorithm for error back-propagation networks," *IEEE Transactions on Signal Processing*, vol. 40, no. 12, pp. 3032-3042, Dec. 1992.

[18] M. Aredes and E. H. Watanabe, "New control algorithms for series and shunt three-phase four-wire active power filters," *IEEE Transactions on Power Delivery*, vol. 10, no. 3, pp. 1649-1656, 1995.

[19] M. J. Ryan, R. W. De Doncker and R. D. Lorenz, "Decoupled control of a four-leg inverter via a new 4×4 transformation matrix," *IEEE Transactions on Power Electronics*, vol. 16, no. 5, pp. 694-701, 2001.

[20] R. R. Sawant and M. C. Chandorkar, "A Multifunctional Four-Leg Grid-Connected Compensator," *IEEE Transactions on Industry Applications*, vol. 45, no. 1, pp. 249-259,2009.

[21] Z. Zeng, H. Yang, J. M. Guerrero and R. Zhao, "Multi-functional distributed generation unit for power quality enhancement," *IET Power Electronics*, vol. 8, no. 3, pp. 467-476,2015.

[22] A. K. Panda and R. Patel, "Adaptive hysteresis and fuzzy logic controlled-based shunt active power filter resistant to shoot-through phenomenon," *IET Power Electronics*, vol.8,no.10,pp.1963-1977,2015.

[23] Y. Karimi, J. M. Guerrero and H. Oraee, "Decentralized method for load sharing and power management in a hybrid single/three-phase islanded microgrid consisting of hybrid source PV/battery units," *2016 IEEE Energy Conversion Congress and Exposition (ECCE)*, Milwaukee, WI,pp.1-8,2016.

[24] Y. Karimi, J. M. Guerrero and H. Oraee, "Decentralized method for load sharing and power management in a hybrid single/three-phase islanded microgrid consisting of hybrid source PV/battery units," *2016 IEEE Energy Conversion Congress and Exposition (ECCE)*, Milwaukee,WI,pp.1-8, 2016.

[25] A. Merabet, K. Tawfique Ahmed, H. Ibrahim, R. Beguenane and A. M. Y. M. Ghias, "Energy Management and Control System for Laboratory Scale Microgrid Based Wind-PV-Battery," *IEEE Transactions on Sustainable Energy*, vol. 8, no. 1, pp. 145-154, 2017.

[26] M. O. Badawy and Y. Sozer, "Power Flow Management of a Grid Tied PV-Battery System for Electric Vehicles Charging," in *IEEE Transactions on Industry Applications*, vol.53,no.2,pp.1347-1357,2017.

[27] A. Mohd *et al*., "Control strategy and space vector modulation for three-leg four-wire voltage source inverters under unbalanced load conditions," in *IET Power Electronics*, vol. 3, no. 3, pp. 323-333, 2010.

[28] Ujjwal Kumar Kalla and Madhuri Mantri, " An Adaptive Control of Voltage Source Converter Based Scheme for Grid connected Solar PV-Battery System," in proc. of *Seventh IEEE Power India International Conference 2016*, pp. 1-6.

[29] B. Singh and S. R. Arya, "Back-Propagation Control Algorithm for Power Quality Improvement Using DSTATCOM," *IEEE Transactions on Industrial Electronics*, vol. 61, no. 3, pp. 1204-1212, March 2014.

[30] B. Subudhi and R. Pradhan, "A comparative study on maximum power point tracking techniques for photovoltaic power systems," *IEEE Trans. on Sustainable Energy*, vol. 4, no. 1, pp. 89-98, , January 2013.

[31] M. Jazayeri, S. Uysal, and K. Jazayeri, "Evaluation of maximum power point tracking techniques in PV systems using MATLAB/Simulink," *Sixth Annual IEEE Green Technologies Conf.*, 2014, pp. 54-60.

Ujjwal Kumar Kalla (SM'16) received his M.Tech Degree. in Power Electronics, Electrical Machines and Drives and Ph.D. from Indian Institute of Technology (IIT) Delhi, India in 2010 and 2015. He is a member of IEEE, Life member of ISTE and Associate member of Institution of Engineers (India). He has received National award of Best M.Tech. Thesis of I.S.T.E. in the year 2010. He is recipient of POSOCO Power System Award of Foundation of Innovation and Technology Transfer, Indian Institute of Technology Delhi and Power System Coorporation in the year 2015. He has received GRIDTECH 2015 award of Power Grid and Ministry of Power, Govt. of India. His areas of interests include Power Electronics, Power Quality, FACTS, Renewable Energy Systems, Active Filters and Electric Machines/Drives.

Hemant Kaushik (S'18) received the B.E. degree in electrical engineering from the University of Rajasthan, Jaipur, India, in 2008, and the M.Tech. degree in power system engineering from Rajasthan Technical University, Kota, India, in 2015. He is currently working toward the Ph.D. degree in electrical engineering with Government Engineering College Bikaner, Bikaner, India. He is a life member of the Indian Society for Technical Education. His research interests include Power Electronics, Power Quality Improvement Techniques, Active Filters and Renewable Energy Systems.

Bhim Singh (SM'99, F'10) received his B.E. in Electrical Engineering from University of Roorkee, India, in 1977 and his M.Tech. and Ph.D. from IIT Delhi, India, in 1979 and 1983. In 1983, he joined Electrical Engineering Department, University of Roorkee, as a Lecturer, and became a Reader in 1988. In December 1990, he joined Electrical Engineering Department, IIT Delhi, as an Assistant Professor. He became an Associate Professor in 1994 and a Professor in 1997. His areas of interest include power electronics, electrical machines and drives, renewable energy systems, active filters, FACTS, HVDC and power quality. Prof. Singh is a Fellow of Indian National Academy of Engineering, National Academy of Sciences, India, Indian Academy of Sciences, Institute of Engineering and Technology, Institution of Engineers (India), and Institution of Electronics and Telecommunication Engineers and a Life Member of Indian Society for Technical Education and System Society of India.

Shailendra Kumar (S'15, M'17) was born in Mahoba, India, in 1988. He received B.Tech. Degree in electrical and electronics engineering from Uttar Pradesh Technical University, Lucknow, India, in 2010, and the M.Tech. Degree in power electronics, electrical machine and drives (PEEMD) from the Indian Institute of Technology, Delhi, India, in 2015. He has completed his Ph.D. degree in department of electrical engineering from the Indian Institute of Technology Delhi, New Delhi, India on 16 May, 2019. Currently, He is working as a Post-Doctoral Research Associate at Khalifa University (Petroleum Institute of Research Centre). His research interests include power quality, grid integration, custom power devices, microgrid and renewable energy. Mr. Kumar is recipient of POSOCO power system award (in Master as well as in Doctoral categories) in 2016 and 2019. He is also a recipient of Prof. SomNathMahendra Student Travel Awards for the PEDES 2018 conference and the IEEE UPCON Best Paper Award in 2016 and 2018.